

Magnetic properties of a mixed spin-3/2 and spin-2 Ising octahedral chain

Xiao-Chen Na(那小晨), Nan Si(司楠), Feng-Ge Zhang(张凤阁), and Wei Jiang(姜伟)
Citation: Chin. Phys. B, 2022, 31 (**8**): 087502. DOI: 10.1088/1674-1056/ac5885
Journal homepage: http://cpb.iphy.ac.cn; http://iopscience.iop.org/cpb

What follows is a list of articles you may be interested in

Magnetic dynamics of two-dimensional itinerant ferromagnet Fe_3GeTe_2

Lijun Ni(倪丽君), Zhendong Chen(陈振东), Wei Li(李威), Xianyang Lu(陆显扬), Yu Yan(严羽), Longlong Zhang(张龙龙), Chunjie Yan(晏春杰), Yang Chen(陈阳), Yaoyu Gu(顾耀玉), Yao Li(黎遥), Rong Zhang(张荣), Ya Zhai(翟亚), Ronghua Liu(刘荣华), Yi Yang(杨燚), and Yongbing Xu(徐永兵)
Chin. Phys. B, 2021, 30 (**9**): 097501. DOI: 10.1088/1674-1056/ac0e25

Electric-field-induced in-plane effective 90° magnetization rotation in Co_2FeAl/PMN-PT structure

Cai Zhou(周偲), Dengyu Zhu(朱登玉), Fufu Liu(刘福福), Cunfang Feng(冯存芳), Mingfang Zhang(张铭芳), Lei Ding(丁磊), Mingyao Xu(许明耀), and Shengxiang Wang(汪胜祥)
Chin. Phys. B, 2021, 30 (**5**): 057504. DOI: 10.1088/1674-1056/abd7de

Evolution of domain structure in Fe_3GeTe_2

Siqi Yin(尹思琪), Le Zhao(赵乐), Cheng Song(宋成), Yuan Huang(黄元), Youdi Gu(顾有地), Ruyi Chen(陈如意), Wenxuan Zhu(朱文轩), Yiming Sun(孙一鸣), Wanjun Jiang(江万军), Xiaozhong Zhang(章晓中), and Feng Pan(潘峰)
Chin. Phys. B, 2021, 30 (**2**): 027505. DOI: 10.1088/1674-1056/abd693

Three- and two-dimensional calculations for the interface anisotropy dependence of magnetic properties of exchange-spring $Nd_2Fe_{14}B/\alpha$-Fe multilayers with out-of-plane easy axes

Qian Zhao(赵倩), Xin-Xin He(何鑫鑫), Francois-Jacques Morvan(李文瀚), Guo-Ping Zhao(赵国平), Zhu-Bai Li(李柱柏)
Chin. Phys. B, 2020, 29 (**3**): 037501. DOI: 10.1088/1674-1056/ab69e9

Magnetization plateaus and frequency dispersion of hysteresis on frustrated dipolar array

Zhang You-Tian
Chin. Phys. B, 2015, 24 (**8**): 087502. DOI: 10.1088/1674-1056/24/8/087502

Magnetic properties of a mixed spin-3/2 and spin-2 Ising octahedral chain

Xiao-Chen Na(那小晨)[1], Nan Si(司楠)[2], Feng-Ge Zhang(张凤阁)[3], and Wei Jiang(姜伟)[2,†]

[1] *School of Science, Shenyang University of Technology, Shenyang* 110870, *China*
[2] *School of Environmental and Chemical Engineering, Shenyang University of Technology, Shenyang* 110870, *China*
[3] *School of Electric Engineering, Shenyang University of Technology, Shenyang* 110870, *China*

(Received 16 January 2022; revised manuscript received 18 February 2022; accepted manuscript online 25 February 2022)

Using an effective field theory with correlations, magnetic properties of an octahedral chain described by a mixed spin Ising model are investigated. Unique phenomena such as multiple hysteresis loops, saturation magnetization, and reverse flip of the magnetization plateaus occur when certain typical parameters are applied. These results may be helpful to further investigate the magnetic properties of one-dimensional systems and could potentially be utilized in the design of spin devices.

Keywords: octahedral chain, magnetization plateaus, hysteresis loops, blocking temperature

PACS: 75.10.Pq, 75.50.Gg, 75.30.Gw **DOI:** 10.1088/1674-1056/ac5885

1. Introduction

At low temperatures, the magnetic and electronic behavior of some chains may exhibit dependence on the value of the spin.[1,2] This phenomenon has garnered tremendous attention as differing behaviors were demonstrated when compared to the bulk matter of the same element.[3,4] Specifically, the focus has been on one-dimensional (1D) magnetic spin chains with transition metal ions due to their inherent magnetic anisotropies and potential application for information storage at the molecular scale.[5–11] Galisova *et al.* investigated the orthogonal-dimer chain using the classical transfer-matrix approach.[12] The results suggested that various ground states lead to six-type magnetization depending on three exchange couplings.

Additionally, the ferromagnetic phase and frustrated ferrimagnetic phase have both been discovered. Based on the Markov property of the dilute Ising chain, Panov obtained an explicit expression for the probability of any finite sequence.[13] He pointed out that the disordered dilute Ising chain with the regular Markov chain, while the ordering gives rise to the irregular Markov chain. Fabrelli *et al.* investigated the spin-1 field-induced antiferromagnet using a combination of experimental and theoretical techniques and delimited the quasi-1D region using quantum Monte Carlo calculations.[14] Das *et al.* synthesized the 1D spin-chain compound $Ca_3Co_{2-x}Fe_xO_6$ and examined its magnetic properties. Some of the low-spin Co^{3+} ions were converted into Co^{2+} ions or, occasionally, both spin states experienced crossover due to the Fe-doping level x.[15] By employing the transfer-matrix method, the ground state phase diagram of spin-1/2 orthogonal-dimer chains has been investigated.[16] Magnetic properties of the quasi-1D spin-1 diamond chain with single-ion anisotropy have also been discussed. The ground state phases exhibited an interesting frustrated state, with the magnetization forming different plateaus.[17] With Monte Carlo simulations, the magnetic properties of the mixed spins-5/2 and 3/2 Ising octahedral chains were investigated.[18] The ground state phase diagrams were determined and the magnetization and magnetic susceptibilities were obtained for this system with several typical anisotropies. If the system is chosen to mixed spins with integer (2) and half-integer (3/2) spins, will the magnetic properties differ from those of only mixed spins with half-integer (5/2,3/2) spins? In this study, we adopt the octahedral chain illustrated in Fig. 1. The blue and purple balls represent the spin-3/2 and 2 magnetic atoms, respectively. The solid and dotted lines depict the nearest neighbor ferromagnetic J (< 0) and ferrimagnetic J_1 (< 0) exchange couplings, respectively. The mixed spin-3/2 and 2 Ising model is employed to introduce the octahedral chain, as this is one of the most effective models for solving one-, two- and three-dimensional problems.[19–22]

To examine this model, an effective field theory (EFT) was employed to analyze the magnetism.[23–26] In our previous studies, we have successfully employed an EFT to study magnetic characteristics of nano-systems.[27–35] The purpose of this study is to investigate the magnetic properties of the octahedral chain described by the mixed spin Ising model based on the EFT. This method takes into account the correlation of spin itself and is therefore superior to mean field theory. In Section 2, the Hamiltonian and a phase transition formula are

†Corresponding author. E-mail: 961463024@qq.com

© 2022 Chinese Physical Society and IOP Publishing Ltd

derived for an octahedral chain using the EFT. In Section 3, the magnetization plateaus, hysteresis loops, and phase diagrams are calculated, while the final section presents some concluding remarks.

2. Calculation method

An octahedral chain with two types of magnetic atoms is depicted in Fig. 1. The initial spins of the blue balls along the magnetic field (h) are anti-parallel to those of the purple balls. The ferromagnetic exchange coupling J is set to unity ($J=1$). Using the EFT, the Hamiltonian for the octahedral chain is

$$\begin{aligned} H &= -J\sum_{ij} S_i^Z S_j^Z - J_1 \sum_{ik} S_i^Z q_k^Z - h\sum_i (S_i^Z + q_k^Z) \\ &\quad - D_1 \sum_i (S_i^Z)^2 - D_2 \sum_k (q_k^Z)^2, \end{aligned} \tag{1}$$

where S_i^Z and q_k^Z represent the spin operators, with possible values $M = (4M_1 + 8M_2 + 4M_3 + M_4 + 4M_5 + 4M_6)/25$ and $\pm 2, \pm 1, 0$, respectively, D_1 (D_2) is the anisotropy of blue (purple) magnetic atoms, and h is the longitudinal magnetic field.

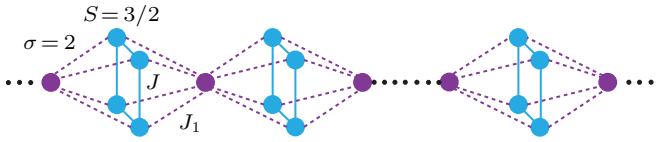


Fig. 1. Schematic of the mixed spin octahedral chain.

The octahedral chain consists of two types magnetic atoms, described by M_a and M_b, which can be calculated by the canonical ensemble average of spin operator. Namely, $S_i(\sigma_m)$ in statistics of spin system is given by $\langle S_i(\sigma_m)\rangle = \langle \mathrm{Tr}_i S_i(\sigma_m)\exp(-\beta H_{i(m)})/\mathrm{Tr}_i \exp(\beta H_{i(m)})\rangle$. Here $\beta = 1/k_B T$, k_B is the Boltzmann constant and T is the absolute temperature. The Hamiltonian $H_{i(m)}$ includes all contributions associated with the site $i(m)$. They are given by EFT as follows:[23–29]

$$\begin{aligned} M_a &= \left[\cosh(J_1\eta_b\nabla) + \frac{M_b}{\eta_b}\sinh(J_1\eta_b\nabla)\right]^2 \\ &\quad \times \left[\cosh(J\eta_a\nabla) + \frac{M_a}{\eta_a}\sinh(J\eta_a\nabla)\right]^2 f_a(x)\,|_{x=0}\,, \end{aligned} \tag{2}$$

$$M_b = \left[\cosh(J_1\eta_a\nabla) + \frac{M_a}{\eta_a}\sinh(J_1\eta_a\nabla)\right]^8 f_b(x)\,|_{x=0}\,, \tag{3}$$

where $\nabla = \partial/\partial x$ is a differential operator, and

$$\begin{aligned} \eta_a^2 &= \left[\cosh(J_1\eta_b\nabla) + \frac{M_b}{\eta_b}\sinh(J_1\eta_b\nabla)\right]^2 \\ &\quad \times \left[\cosh(J\eta_a\nabla) + \frac{M_a}{\eta_a}\sinh(J\eta_a\nabla)\right]^2 g_a(x)\,|_{x=0}\,, \end{aligned} \tag{4}$$

$$\eta_b^2 = \left[\cosh(J_1\eta_a\nabla) + \frac{M_a}{\eta_a}\sinh(J_1\eta_a\nabla)\right]^8 g_b(x)\,|_{x=0}\,, \tag{5}$$

where η_a and η_b are defined as $\eta_a^2 = \langle (S_i^z)^2\rangle$ and $\eta_b^2 = \langle (\sigma_m^z)^2\rangle$. They are intermediate parameters for the sublattice magnetizations. Usually, the thermal behavior of these parameters need not be discussed.

The total average magnetization per site M is defined by

$$M = (4M_a + M_b)/5. \tag{6}$$

The functions $f_a(x)$, $g_a(x)$ and $f_b(x)$, $g_b(x)$ can be written as

$$f_a(x) = \frac{3\sinh\left[\frac{3}{2}\beta x\right] + \exp(-2D_1\beta)\sinh\left[\frac{1}{2}\beta x\right]}{2\cosh\left[\frac{3}{2}\beta x\right] + 2\exp(-2D_1\beta)\cosh\left[\frac{1}{2}\beta x\right]}, \tag{7}$$

$$g_a(x) = \frac{9\cosh\left[\frac{3}{2}\beta x\right] + \exp(-2D_1\beta)\cosh\left[\frac{1}{2}\beta x\right]}{4\cosh\left[\frac{3}{2}\beta x\right] + 4\exp(-2D_1\beta)\cosh\left[\frac{1}{2}\beta x\right]}, \tag{8}$$

$$f_b(x) = \frac{4\sinh[2\beta x] + 2\exp(-3D_2\beta)\sinh[\beta x]}{2\cosh[2\beta x] + 2\exp(-3D_2\beta)\cosh\left[\frac{1}{2}\beta x\right] + \exp(-4D_2\beta)}, \tag{9}$$

$$g_b(x) = \frac{8\sinh[2\beta x] + 2\exp(-3D_2\beta)\sinh[\beta x]}{2\cosh[2\beta x] + 2\exp(-3D_2\beta)\cosh\left[\frac{1}{2}\beta x\right] + \exp(-4D_2\beta)}. \tag{10}$$

The average magnetic susceptibility is given by

$$\chi = \frac{\partial M}{\partial h}\,|_{h=h_0}. \tag{11}$$

3. Numerical results and discussion

In this section, some typical results based on the magnetic properties of the octahedral chain described by the ferrimagnetic mixed Ising model are investigated. Suppose that the spin-3/2 at the blue sites is parallel to the magnetic field (h), while the spin-2 at the purple sites is anti-parallel and the ferromagnetic exchange coupling is set to unity.

3.1. Magnetization plateaus and hysteresis loops of the octahedral chain

The step effects exhibited at low temperatures by the magnetization of the system with an increasing magnetic field are known as magnetization plateaus. Generally, the number of plateaus depends on the values of spin and other parameters. The effects of the exchange coupling J_1 and anisotropies

D_1 and D_2 on the octahedral chain are examined in Figs. 2–4 at a fixed temperature of $T = 0.06$. The solid, dashed, and dot-dashed lines denote the total average (M), A (M_a) and B (M_b) sublattice magnetizations, respectively.

The magnetization versus the magnetic field for the octahedral chain with $D_1 = -0.5$, $D_2 = -3.5$ and various values of J_1 are depicted in Figs. 2(a) and 2(b). In these figures, magnetization plateaus are observed at the curves. The critical magnetic field h_c is defined as the smallest magnetic field required for the magnetization to transition from one plateau to another, while that of the last plateau is known as the saturated magnetic field h_s. In Fig. 2(a), three magnetization plateaus are observed at $M = 6/5$, 7/5, and 8/5 with $J_1 = -0.2$, corresponding to $h_{c1} = 6.26$ and $h_s = 13.36$, respectively. The sublattice M_a remains constant for the spin 3/2 state, while M_b moves from a 0 to a +2 spin state as h increases. The magnetization plateaus are sensitive to sublattice plateaus, such as $M = [4 \times (3/2) + 0]/5 = 6/5$. In Fig. 2(b), four magnetization plateaus are observed at $M = 1$, 6/5, 7/5, and 8/5 with $J_1 = -0.7$, corresponding to $h_{c1} = 5.26$, $h_{c2} = 12.26$, and $h_s = 19.36$, respectively. The spin of M_b moves from a -1 to a +2 state as h increases, which differs from the previous example. An additional plateau was observed due to $M = [4 \times (3/2) + (-1)]/5 = 1$. Comparing Fig. 2(a) and Fig. 2(b), the values of h_c and h_s for the same plateau increase with the increasing $|J_1|$.

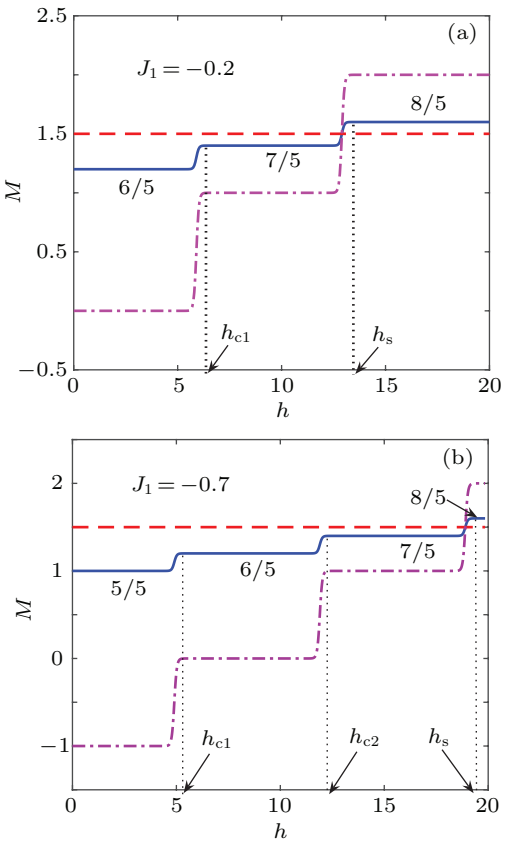


Fig. 2. Magnetization plateaus of the octahedral chain with various J_1: (a) −0.2 and (b) −0.7.

The magnetization against magnetic field for the octahedral chain with $J_1 = -0.7$ and $D_2 = -3.5$ for various D_1 are presented in Figs. 3(a) and 3(b). In Fig. 3(a), four magnetization plateaus are observed at $M = 1$, 6/5, 7/5, and 8/5 with $D_1 = -1.5$, corresponding to $h_{c1} = 5.26$, $h_{c2} = 12.26$, and $h_s = 19.36$, respectively. In Fig. 3(b), six magnetization plateaus are observed at $M = -2/5$, 2/5, 3/5, 6/5, 7/5, and 8/5 with $D_1 = -4.5$, corresponding to $h_{c1} = 0.54$, $h_{c2} = 6.8$, $h_{c3} = 9.1$, $h_{c4} = 12.26$, and $h_s = 19.26$, respectively. Interestingly, M_b is inverted from 1 to 0, while M_a moves from spin 1/2 to spin 3/2 at h_{c3}. This phenomenon arises due to the opposite directions of the initial spins of the two types of sublattices (M_a and M_b) owing to the ferrimagnetic exchange coupling ($J_1 < 0$). To retain this ferrimagnetic exchange coupling, they must change simultaneously. That is, M_a and M_b simultaneously move up and down, respectively. Comparing the two cases, the critical magnetic fields increase with the increasing $|D_1|$ for the same plateau under lower magnetic fields. However, the saturated magnetic field h_s retains the same value. The corresponding plateaus are similar for both the cases, for example, $M = (4 \times 3/2 - 0)/5 = 6/5$ for both $D_1 = -1.5$ and -4.5.

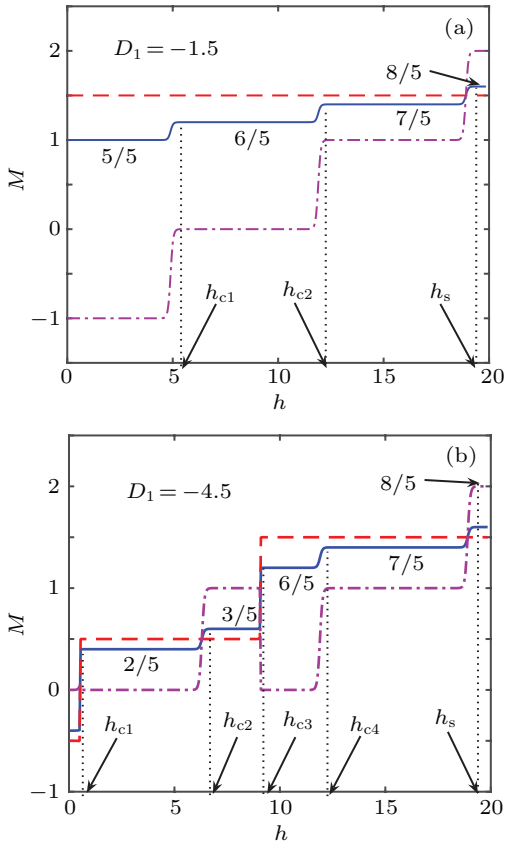


Fig. 3. Magnetization plateaus of the octahedral chain for various D_1: (a) −1.5 and (b) −4.5.

The magnetization versus magnetic field for the octahedral chain with $J_1 = -0.7$ and $D_1 = -0.5$ for various values of D_2 is illustrated in Figs. 4(a) and 4(b). In Fig. 4(a), five magnetization plateaus are observed from five spin states, −2, −1,

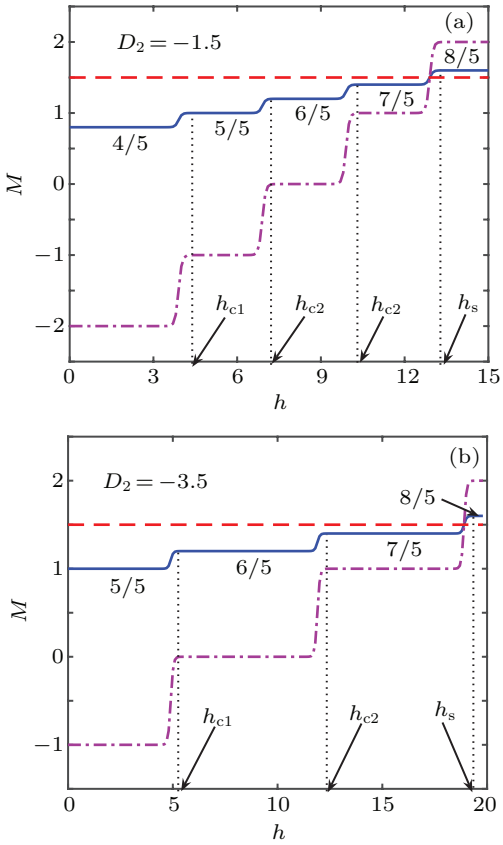


Fig. 4. Magnetization plateaus of the octahedral chain for various D_2: (a) -1.5, (b) -3.5.

0, 1, and 2 for M_b. They are observed at $M = 4/5$, 5/5, 6/5, 7/5, and 8/5 for $D_2 = -1.5$, corresponding to $h_{c1} = 4.4$, $h_{c2} = 7.26$, $h_{c3} = 10.26$, and $h_s = 13.26$, respectively. In Fig. 4(b), four magnetization plateaus are observed at $M = 5/5$, 6/5, 7/5, and 8/5 for $D_2 = -3.5$, corresponding to $h_{c1} = 5.26$, $h_{c2} = 12.26$, and $h_s = 19.26$, respectively. Comparing the two figures, one of the lowered plateaus is due to the absence of the -2 spin state in M_b. The multi-spin states of the system are sensitive to various parameters, stronger anisotropy makes the system in a low spin state, whereas weaker one makes it in a high spin state. This results in a different number of magnetization plateaus.

Figures 5(a)–5(d) demonstrate the effect of the ferrimagnetic exchange coupling J_1 on the magnetic hysteresis loops and the coercivity of the octahedral chain with $D_1 = -0.5$ and $D_2 = -3.5$ at a fixed temperature $T = 0.06$. With increasing h, the curve saturates at $M_s = 8/5$ in Fig. 5(a), where $J_1 = -0.2$. The coercivity and the remanence are $H_c = 2.16$ and $M_r = 6/5$, respectively. To explain the origin of the overall hysteresis loops, the magnetic hysteresis loops of the sublattices are plotted in Fig. 5(b) with the same parameters. M_a and M_b exhibit different dependencies for various values of h, which determines the shape of the overall hysteresis loop. They also account for the source of $M_s = (4 \times 3/2 + 2)/5 = 8/5$. In Fig. 5(c), where $J_1 = -0.7$, the coercivity and the remanence are $H_c = 2.26$ and $M_r = 5/5$, respectively. In comparison of the two cases, H_c is observed to increase when the absolute value of J_1 increased from 0.2 to 0.7. Additionally, the coercivity H_c versus J_1 in Fig. 5(d) further confirms the above result.

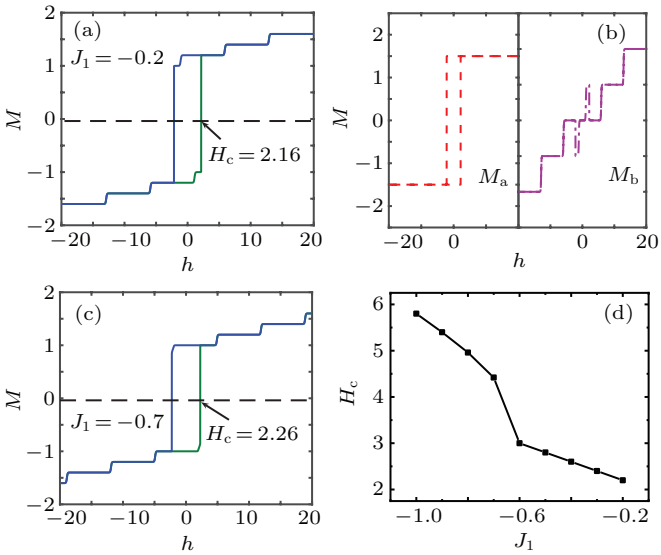


Fig. 5. Hysteresis loops of the octahedral chain for (a) $J_1 = -0.2$, (b) $J_1 = -0.2$ for the sublattices, (c) $J_1 = -0.7$, and (d) the coercivity H_c versus J_1.

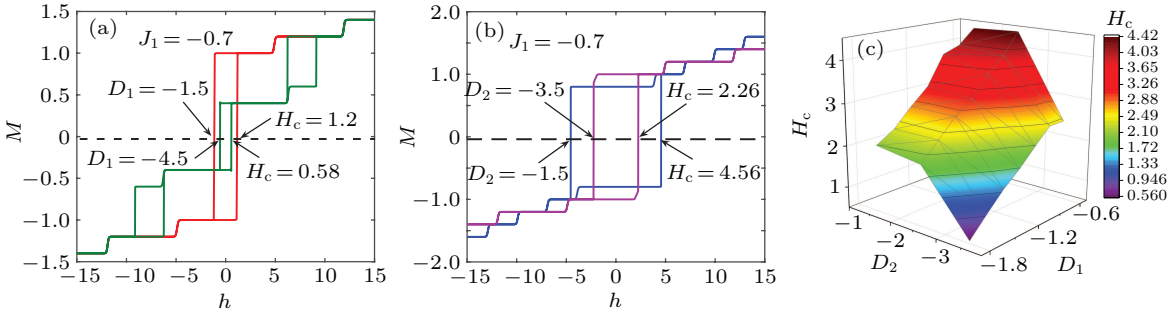


Fig. 6. Hysteresis loops for (a) $D_2 = -3.5$, $D_1 = -1.5$ and -4.5, (b) $D_1 = -0.5$, $D_2 = -1.5$ and -3.5, and the coercivity H_c, and (c) the three-dimensional space (H_c, D_2, D_1) of the octahedral chain.

The graphs in Figs. 6(a)–6(c) explain the effects of the anisotropies on the magnetic hysteresis loops and the coercivity of the octahedral chain for $J_1 = -0.7$ and $T = 0.06$. In Fig. 6(a), the coercivity and the remanence are $H_c = 1.2$ and 0.58, and $M_r = 5/5$ and 2/5 for $D_1 = -1.5$ and -4.5, respectively, for a fixed anisotropy of $D_2 = -3.5$. Moreover,

three loops are found on the curve where $D_1 = -4.5$, which is due to all possible spin states appearing with the increasing magnetic field. In Fig. 6(b), the coercivity and the remanence are $H_c = 2.26$ and 4.56, and $M_r = 5/5$ and 4/5 for $D_2 = -3.5$ and -1.5, respectively, for a fixed anisotropy of $D_1 = -0.5$. The steps are observed on the hysteresis loops due to all possible spin states appearing with the increasing magnetic field. The effects of the anisotropies on the coercivity in the three-dimensional space (H_c, D_2, D_1) of the octahedral chain are given in Fig. 6(c). The hysteresis loop and magnetization plateaus are mainly caused by the multi-spin states of 1D ferrimagnetic system due to the anisotropy, which may have potential applications in magnetic memory devices.

3.2. Magnetization and blocking temperature of the octahedral chain

The curves in Figs. 7(a)–7(c) depict the effects of the ferrimagnetic exchange J_1 on the magnetizations and the susceptibility of the octahedral chain for $D_1 = -0.5$ and $D_2 = -3.5$. In Fig. 7(a), the temperature dependence of the magnetization is plotted for some typical values of J_1. The depressed saturation magnetization is observed on the curves labeled $J_1 = -0.4$, as the thermal agitation releases the saturation magnetization from the frustration. In Fig. 7(b), three saturation magnetizations (M_s) at zero temperature are detected at $M_s = 6/5$, 5/5, and 4/5, which arise from $M_s = (4 \times 3/2 - 0)/5 = 6/5$, $(4 \times 3/2 - 1)/5 = 5/5$, and $(4 \times 3/2 - 2)/5 = 4/5$. The saturation sublattice magnetization labeled $J_1 = -0.9$, -0.7 at zero temperature showed smaller than the absolute value of the maximum M_b due to its released from the frustration through thermal agitation. In Fig. 7(c), the temperature dependence of the susceptibility of the octahedral chain is analyzed using the same parameters as shown in Fig. 7(a). The temperature at maximum susceptibility is defined as the blocking temperature (T_B), and we observe that with increasing $|J_1|$, T_B also increases. For example, $T_c = 2.35$, 2.7, 3.7, 4.5, and 6.1 for $J_1 = -0.2$, -0.4, -0.7, -0.9, and -1.2, respectively. The blocking temperature (T_B) as a function of the ferrimagnetic exchange coupling J_1 is presented in Fig. 7(d) for $D_1 = -0.5$ and $D_2 = 2.5$. It is observed that T_B decreases with decreasing $|J_1|$, which agrees with the previous analysis.

The curves in Figs. 8(a)–8(c) depict the effects of the anisotropy D_1 on the magnetization and the susceptibility of the octahedral chain for $J_1 = -0.7$ and $D_2 = -3.5$. In Fig. 8(a), the temperature dependence of the magnetization of the system is given for some typical values of D_1. Two values of M_s are found on the total average magnetization at $M_s = 5/5$ and 2/5. The different types of magnetization curves are due to the different temperature dependences of M_a and M_b in Fig. 8(b). The saturation magnetizations are $M_s = 3/2$ and $1/2$, and 0 and -1 for M_a and M_b, respectively. This originates from the different magnetic states induced by anisotropy changes. In Fig. 8(c), the temperature dependence of the susceptibility of the octahedral chain is analyzed with the same parameters as shown in Fig. 8(a). The singular behavior is observed at T_B on the curve, at which point the temperature increases with decreasing $|D_1|$. For example, $T_B = 3.4$, 2.9, 2.3, 1.5, and 0.8 for $D_1 = -0.8$, -1.2, -1.5, -2.3, and -4.5, respectively.

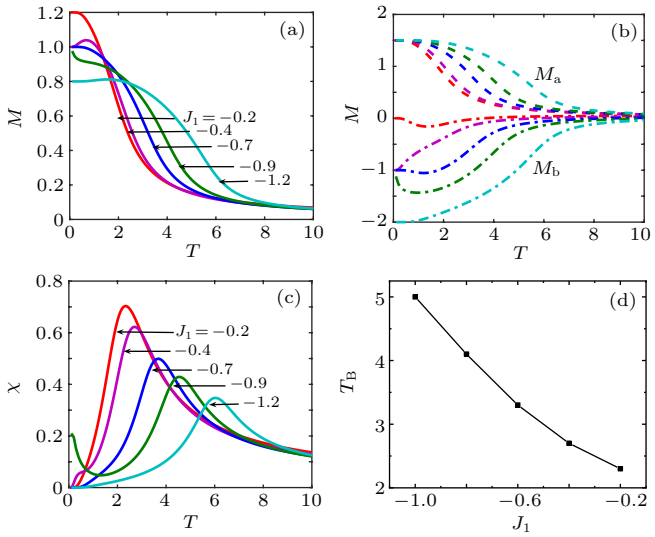


Fig. 7. Temperature dependence of the (a) magnetization, (b) sublattice magnetization, (c) susceptibility, and (d) the blocking temperature T_B vs. J_1 of the octahedral chain for $D_1 = -0.5$, $D_2 = -3.5$.

The curves in Figs. 9(a)–9(c) describe the effects of the anisotropy D_2 on the magnetization and the susceptibility of the octahedral chain with $J_1 = -0.7$ and $D_1 = -0.5$. In Fig. 9(a), the temperature dependence of the magnetization of the system is plotted for some typical values of D_2. Two values of M_s are observed at $M_s = 5/5$ and 4/5. The different types of magnetization curves are due to the dependence of the various sublattice magnetizations on temperature, as illustrated in Fig. 9(b). The saturation magnetizations are $M_s = 3/2$, and -2 and -1 for M_a and M_b, respectively. In Fig. 9(c), the temperature dependence of the susceptibility of the octahedral chain is analyzed with the same parameters as shown in Fig. 9(a). The singular point on the curve at T_B increases with decreasing $|D_2|$. For example, $T_B = 3.7$, 3.9, 4.1, 4.6, and 5.2 for $D_2 = -3.5$, -3.0, -2.5, -1.5, and -0.2, respectively. The susceptibility curve also contains an additional peak at low temperature due to the depressed saturation magnetization. The effects of the anisotropies on the blocking temperature are plotted in Figs. 9(d) and 9(e) for $J_1 = -0.7$. In Fig. 9(d), the blocking temperature dependence of the anisotropy D_1 of the system is plotted for some typical values of D_2. For the same parameters, T_B agrees with that obtained in Fig. 9(c). To clearly show the variation of the blocking temperature with anisotropy, a three-dimensional space (T_B, D_1, D_2) is provided for the octahedral chain.

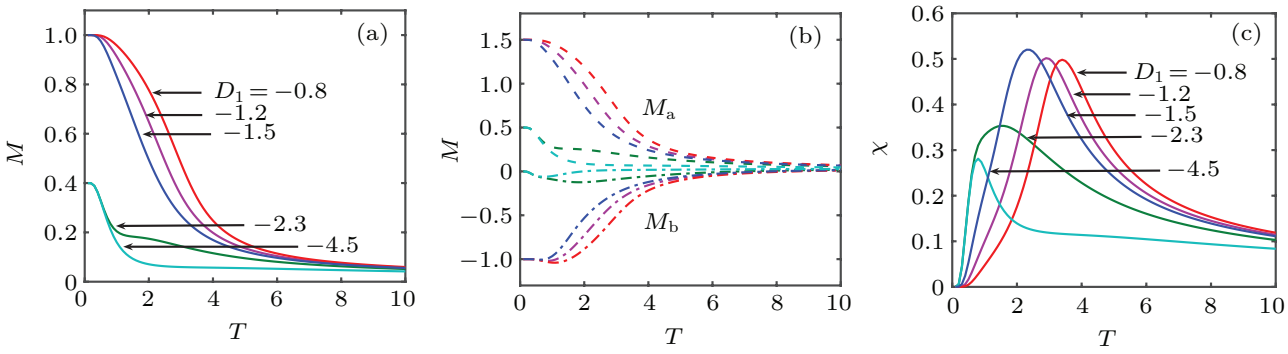


Fig. 8. Temperature dependence of (a) magnetization, (b) sublattice magnetization, and (c) susceptibility for the octahedral chain with $J_1 = -0.7$ and $D_2 = -3.5$. The number on the curve is the anisotropy D_1.

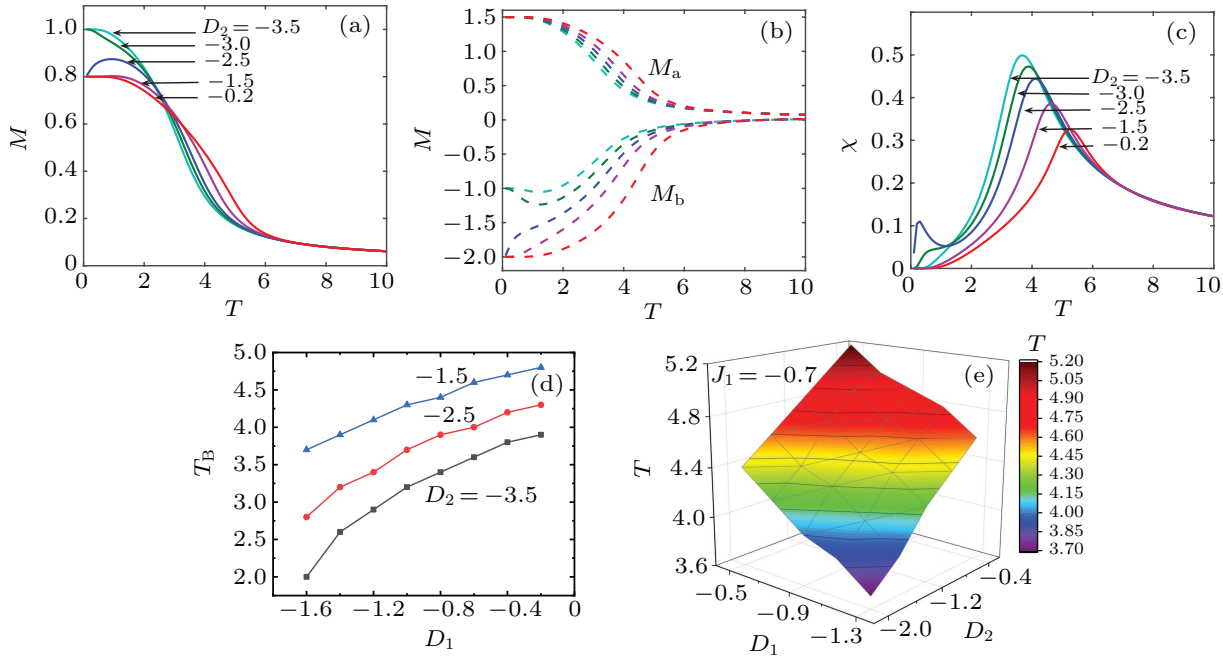


Fig. 9. Temperature dependence of (a) magnetization, (b) sublattice magnetization, and (c) susceptibility with $J_1 = -0.7$ and $D_1 = -0.5$, and the blocking temperature in (d) two-dimensional (T_B, D_1) and (e) three-dimensional space (T_B, D_1, D_2) for the octahedral chain.

4. Conclusions

An octahedral chain described using a mixed spin Ising model has been investigated within the framework of an EFT with correlations. The calculations demonstrate that the exchange coupling and anisotropy exhibit important impacts on magnetism. For appropriate parameters, depressed saturation magnetization may be obtained in such a system. Furthermore, unusual behaviors, such as multiple hysteresis loops with the step effect and magnetization plateau inversion, have been discovered. These behaviors in 1D materials may be applicable to spin devices in the future.

Acknowledgements

Project supported by National Natural Science Foundation of China (Grant No. 51920105011) and the Key R&D Program of Liaoning Province of China (Grant No. 2020JH2/10300079).

References

[1] Coronado E, Galan-Mascaros J R and Marti-Gastaldo C 2008 *J. Am. Chem. Soc.* **130** 14987
[2] Zhao Y, Qi Y, Du A, Liu J, Xiao R, Shan Y, Wu Y and Yang S H 2017 *Acta Phys. Sin.* **66** 197501 (in Chinese)
[3] Qiu M S, Guo H H, Zhang Y, Dong B J, Ali S and Yang T 2019 *Chin. Phys. B* **28** 106103
[4] Yang T, Okano S, Berber S and Tomanek D 2006 *Phys. Rev. Lett.* **96** 125502
[5] Colacio E, Ruiz J, Ruiz E, Cremades E, Krzystek J, Carretta S, Cano J, Guidi T, Wernsdorfer W and Brechin E K 2013 *Angew. Chem. Int. Edit.* **52** 9130
[6] Kageyama H, Yoshimura K and Kosuge K 1998 *J. Solid State Chem.* **140** 14
[7] Liu T F, Fu D, Gao S, Zhang Y Z, Sun H L, Su G and Liu Y J 2003 *J. Am. Chem. Soc.* **125** 13976
[8] Clerac R, Miyasaka H, Yamashita M and Coulon C 2002 *J. Am. Chem. Soc.* **124** 12837
[9] Lescouezec R, Vaissermann J, Ruiz-Perez C, Lloret F, Carrasco R, Julve M, Verdaguer M, Dromzee Y, Gatteschi D and Wernsdorfer W 2003 *Angew. Chem.* **42** 1483
[10] Kageyama H, Yoshimura K and Kosuge K 1998 *J. Solid State Chem.* **140** 14
[11] Zheng G P, Liang J Q and Liu W M 2009 *Phys. Rev. B* **79** 014415

[12] Galisova L, Strecka J, Verkholyak T and Havadej S 2021 *Physica E* **125** 114089
[13] Panov Y D 2020 *J. Magn. Magn. Mater.* **514** 167224
[14] Fabrelli H, Vieira A P, Paduan A and Freitas R S 2021 *J. Alloy. Compd.* **853** 157346
[15] Das R, Dang N T, Kalappattil V, Madhogaria R P, Kozlenko D P, Kichanov S E, Lukin E V, Rutkaukas A V, Thao T P T, Nguyen L T P, Bingham N S, Srikanth H and Phan M H 2021 *J. Alloys Compd.* **851** 156897
[16] Galisova L, Strecka J, Verkholyak T and Havadej S 2021 *Physica E* **125** 114089
[17] Abgaryan V S, Ananikian N S, Ananikyan L N and Hovhannisyan V V 2015 *Solid State. Commun.* **224** 15
[18] Jabar A and Masrour R 2018 *Spin* **8** 1850017
[19] Zhang Z D 2007 *Philos. Mag.* **87** 5309
[20] Zhang Z D 2013 *Chin. Phys. B* **22** 030513
[21] Žukovič M and Bobák A 2015 *Physica A* **436** 509
[22] Zhang Z D, Suzuki O and March N H 2019 *Adv. Appl. CClifford Algebras* **29** 12
[23] Barreto F C S and Zeks I P F B 1981 *Ferroelectrics* **39** 1103
[24] Sarreto B F C and Fittipaldi I P 1985 *Physica A* **129** 360
[25] Kaneyoshi T, Tucker J W and Jascur M 1992 *Physica A* **186** 495
[26] Kaneyoshi T 2019 *Physica B* **561** 141
[27] Si N, Wang J M, Guo A B, Zhang F, Zhang F G and Jiang W 2020 *Physica E* **118** 113884
[28] Si N, Su X, Meng J, Miao H L, Zhang Y L and Jiang W 2020 *Physica A* **560** 125222
[29] Zhang F, Zhang F G, Liu S Q, Meng J, Miao H L and Jiang W 2020 *Chin. J. Phys.* **66** 390
[30] Jiang W, Wang Y N, Guo A B, Yang Y Y and Shi K L 2016 *Carbon* **110** 41
[31] Si N, Zhang F, Jiang W and Zhang Y L 2018 *Physica A* **510** 641
[32] Quan X W, Si N, Zhang F, Meng J, Miao H L, Zhang Y L and Jiang W 2019 *Physica E* **114** 113574
[33] Hu J Q, Si N, Wang J, Meng J and Zhang Y L 2021 *Phys. Lett. A* **405** 127434
[34] Si N, Zhang Y L and Jiang W 2021 *Comput. Mater. Sci.* **197** 110594
[35] Si N, GuaY Y, Gao W C, Guo A B, Zhang Y L and Jiang W 2022 *Physica A* **589** 126671